

PILOT-IN-THE-LOOP SIMULATION OF OPTIMAL DEEP-STALL RECOVERY FOR T-TAIL AIRLINER

Koki Yoshioka[1] & Takeshi Tsuchiya[1]

[1]The University of Tokyo, Tokyo, 113-8656, Japan, koki-yoshioka@g.ecc.u-tokyo.ac.jp

Abstract

Pilot-in-the-loop simulations were conducted to evaluate the recovery control from the deep-stall equilibrium of a T-tail airliner. The optimal inputs were obtained via an optimal control problem. The solution utilizes the coupling of longitudinal and lateral dynamics to reduce the angle of attack. In the real-time simulator experiments, the optimal inputs were given to the pilot as text instructions or were automatically executed. Without the instructions or execution, the pilot failed to recover from deep stall. The text instructions enabled stall recovery, but the pilot workload was high. The automatic execution reduced the pilot workload and altitude loss in stall recovery.

Keywords: Deep stall, Optimal control, Pilot-in-the-loop simulation, Upset recovery

1. Introduction

In the dynamics of a T-tail airliner, there may exist two stable equilibrium points corresponding to deep stall and level flight. Recovery from the deep stall equilibrium remains difficult due to its stability and the loss of elevator control authority [1, 2, 3, 4]. Previous studies have proposed a method called pitch rocking, in which periodic and resonant elevator inputs generate sufficient angular momentum in the pitch direction to reduce the angle of attack [5, 6]. Recent research has advanced this method by analyzing the nonlinear frequency response of the longitudinal system [1]. In contrast, we have proposed optimization of both longitudinal and lateral control inputs within the six-degree-of-freedom system to obtain more rapid recovery method [3, 4].

As mentioned above, research on deep stall recovery has progressed in recent years. For practical implementation, its effectiveness must be evaluated through pilot-in-the-loop simulations. Among pitch rocking methods, an approach in which the pilot empirically matches the input frequency to the resonance frequency has been evaluated through simulator experiments [5]. The optimal control that we have proposed also requires experimental evaluation.

In this study, first, we solve an optimal control problem in which the required time and altitude loss are considered in the objective function. Then, based on the optimal input, we conduct three cases of simulator experiments: pattern 1 (manual input without instructions), pattern 2 (manual input with text instructions), and pattern 3 (automatic input). From the results, we evaluate the effectiveness of the proposed recovery control.

2. Aircraft Model

The equations of motion can be expressed as the following nonlinear dynamical system [7].

$$\begin{aligned} \dot{\boldsymbol{x}} &= \boldsymbol{f}(\boldsymbol{x}, \boldsymbol{u}) \\ \boldsymbol{x} &= [z_e, \phi, \theta, U, V, W, P, Q, R]^T \\ \boldsymbol{u} &= [\delta_r, \delta_a, \delta_e]^T \end{aligned} \tag{1}$$

Here, z_e denotes z coordinate in the Earth-fixed frame, ϕ, θ are Euler angles, U, V, W are translational velocities, and P, Q, R are angular velocities. Inputs are rudder δ_r, ailerons δ_a, and elevator δ_e. The positive direction is rudder trailing edge left, right aileron trailing edge down, and elevator trailing edge down.

The model discussed in this study is based on the NASA generic transport model (GTM), a 5.5 % scaled model of a passenger aircraft [8]. To reproduce the behavior of full-scale aircraft, scale effects are reflected to the properties of the GTM such as mass or moment of inertia. Since the GTM has a conventional tail configuration, the longitudinal aerodynamic coefficients C_L, C_D, C_m are replaced with those of Lear Jet 23 [9], known for its deep stall tendency with a T-tail configuration [2]. The ranges of control surface deflection are based on those of the GTM [10] and Lear Jet 23 [9].

$$-45 < \delta_r < 45 \text{ deg}, \ -30 < \delta_\text{a} < 30 \text{ deg}, \ -15 < \delta_\text{e} < 15 \text{ deg} \tag{2}$$

In optimization, we use the state variables at the GTM scale, whereas in simulator experiments, the variables are converted into the full-scale values using the following relationships [11]. Here, the scale factor $k = 0.055$ [8].

$$\begin{cases} t_\text{full} = \dfrac{1}{\sqrt{k}} t_\text{GTM} \simeq 4.26 t_\text{GTM} \\ [X_e, Y_e, Z_e]^T{}_\text{full} = \dfrac{1}{k} [X_e, Y_e, Z_e]^T{}_\text{GTM} \simeq 18.2 [X_e, Y_e, Z_e]^T{}_\text{GTM} \\ [\phi, \theta, \psi]^T{}_\text{full} = [\phi, \theta, \psi]^T{}_\text{GTM} \\ [U, V, W]^T{}_\text{full} = \dfrac{1}{\sqrt{k}} [U, V, W]^T{}_\text{GTM} \simeq 4.26 [U, V, W]^T{}_\text{GTM} \\ [P, Q, R]^T{}_\text{full} = \sqrt{k} [P, Q, R]^T{}_\text{GTM} \simeq 0.235 [P, Q, R]^T{}_\text{GTM} \\ [\delta_r, \delta_a, \delta_e]^T{}_\text{full} = [\delta_r, \delta_a, \delta_e]^T{}_\text{GTM} \end{cases} \tag{3}$$

Note that the air density ρ is assumed constant, and the thrust is fixed at the value required for the level flight of the GTM.

3. Optimal Control Problem

3.1 Formulation

The optimal control problem is formulated as follows:

Minimize

$$J = t_\text{f}^2 + k_w z_{e,\text{f}}^2 \tag{4}$$

Subject to

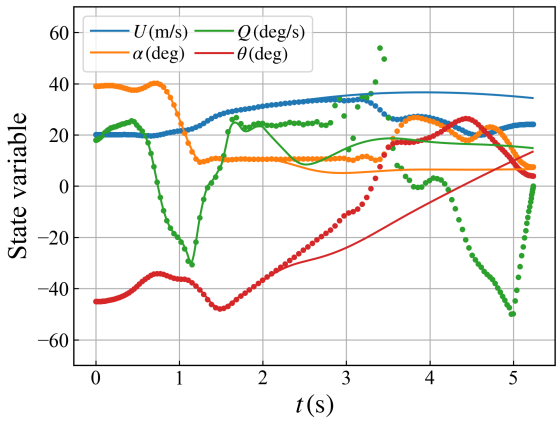
$$\dot{\boldsymbol{x}} = \boldsymbol{f}(\boldsymbol{x}, \boldsymbol{u}) \tag{5}$$

$$\boldsymbol{x}_0 = \boldsymbol{x}_\text{ini} \tag{6}$$

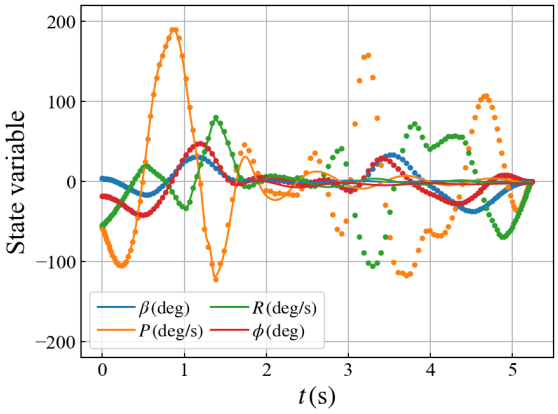
$$\boldsymbol{x}_\text{f} = \boldsymbol{x}_e \tag{7}$$

$$\boldsymbol{u}_\text{min} < \boldsymbol{u} < \boldsymbol{u}_\text{max} \tag{8}$$

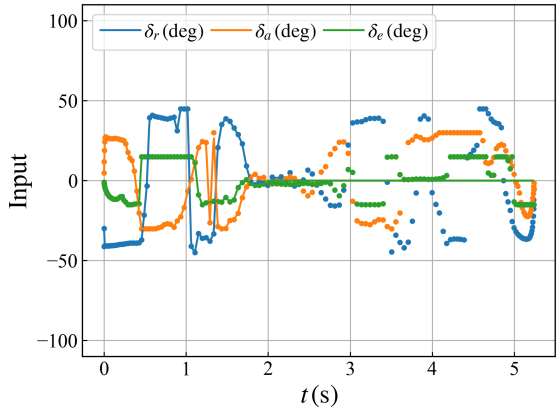
Here, the subscript 0 denotes the value at the initial time, and the subscript f denotes the value at the final time. $\boldsymbol{x}_\text{ini}$ is the specified initial state, which is the stable equilibrium point with deep stall. $\boldsymbol{x}_e$ is the target equilibrium point, the steady level flight. (The specific values of these equilibrium points are given in Appendix.) k_w is the weight. The optimization variables are the final time t_f, the state variable $\boldsymbol{x}(t)$, and the control input $\boldsymbol{u}(t)$. This optimal control problem is discretized in the time domain using the Legendre-Gauss pseudospectral method [12, 13]. This results in nonlinear programming (NLP). The NLP is solved by IPOPT [14]. The initial guess provided to the solver is as follows. The state $\boldsymbol{x}$ is linear interpolation between $\boldsymbol{x}_\text{ini}$ and $\boldsymbol{x}_e$. The input $\boldsymbol{u} = \boldsymbol{0}$. The final time $t_\text{f} = 1.0$ s.



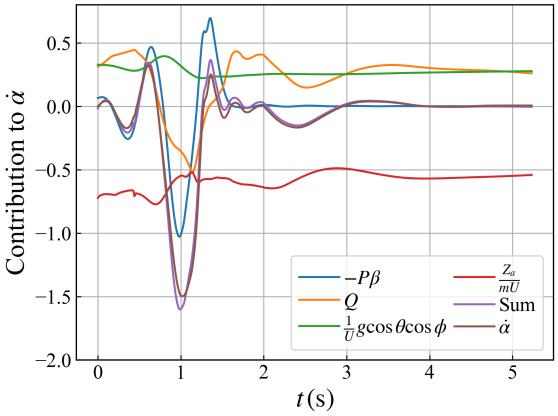
(a) Longitudinal state variables.



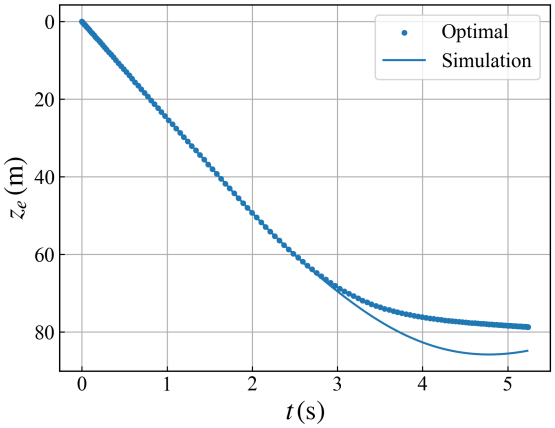
(b) Lateral state variables.



(c) Control inputs.



(d) Contribution to $\dot{\alpha}$.



(e) z coordinate in the Earth-fixed frame.

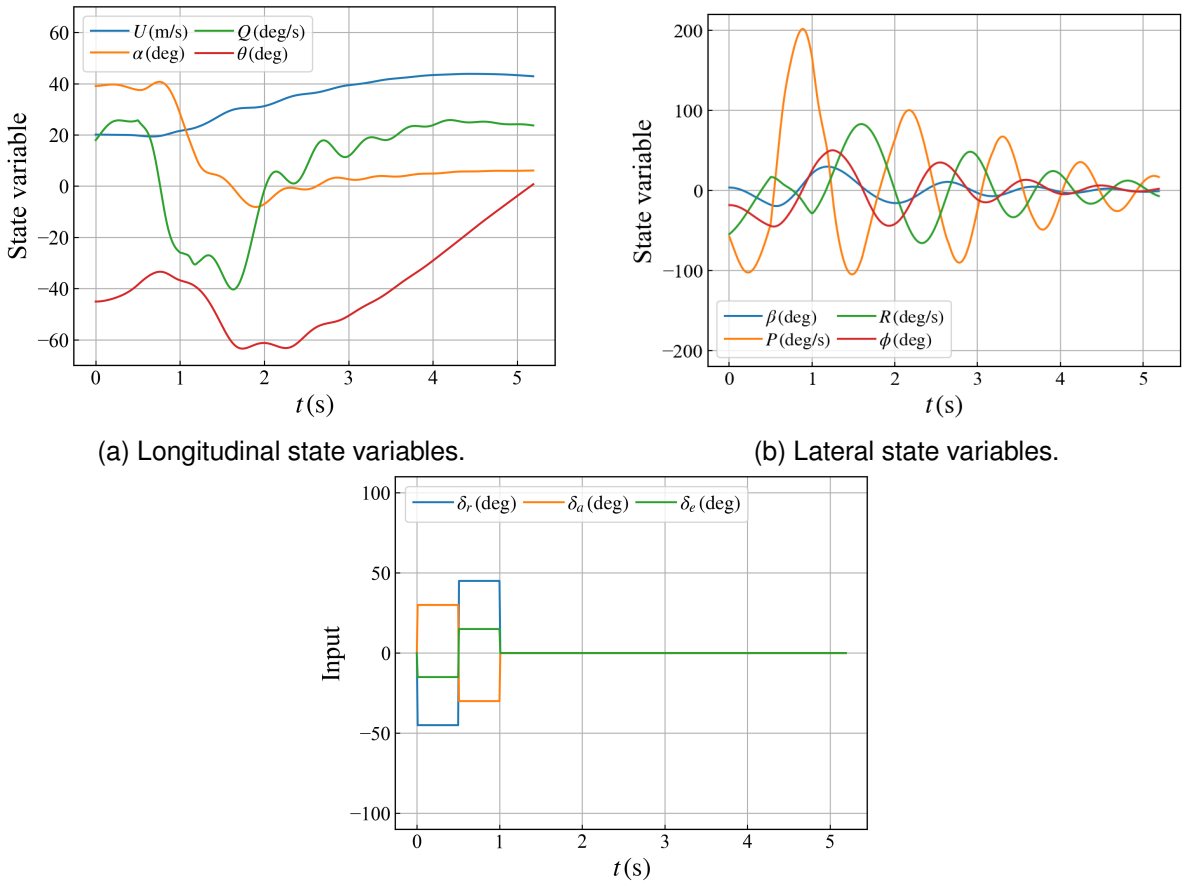
Figure 1 – Optimal recovery with 150 collocation points (at GTM scale).

3.2 Optimization Result

Figure 1 shows the result with 150 collocation points (discrete points in the time domain). The discrete markers represent the optimization results, while the continuous lines show the result of the continuous-time simulation using the optimal input up to $t = 2.0$ s. Before $t = 2.0$ s, the angle of attack α decreases and the lateral state variables almost converge to zero. The subsequent free response exhibits symmetric phugoid motion at low angle of attack. On the other hand, the optimal solution after $t = 2.0$ s utilizes re-stall to pitch up. Thus, this part of the optimal solution is not adopted.

Following our previous studies [4, 3], approximating $\alpha \simeq W/U$ and $\beta \simeq V/U$ yields the approximate expression for $\dot{\alpha}$ as follows:

$$\dot{\alpha} \simeq -P\beta + Q + \frac{1}{U} g \cos\theta \cos\phi + \frac{Z_a}{mU} \tag{9}$$



(a) Longitudinal state variables.

(b) Lateral state variables.

(c) Control inputs.

Figure 2 – Simulation result with approximated bang-bang inputs (at GTM scale).

In Fig. 1d, the sum of the terms on the right-hand side is close to $\dot{\alpha}$, which demonstrates the validity of Eq. (9). Comparing the contribution of each term to $\dot{\alpha}$, $-P\beta$ is the largest at $t = 1.0$ s. This indicates that the coupling of longitudinal and lateral dynamics enables the reduction of the angle of attack. This is interpreted as follows. In a deep stall condition, the control authority of elevator δ_e is lost. Thus, the rudder δ_r and ailerons δ_a induce the side slip angle β and roll rate P. The term $-P\beta$ means that β is converted into α with P [4, 3].

3.3 Approximation to Bang-Bang Inputs

The optimal input shown in Fig. 1c seems too complex to be presented as instructions to a pilot in simulator experiments. Therefore, we approximate the optimal input up to $t = 1.0$ s as bang-bang inputs. The switching time is $t = 0.5$ s. Figure 2 shows the simulation result with the bang-bang inputs. The angle of attack α decreases and the lateral state variables approach zero. Stall recovery is still achieved, and the aircraft enters nearly symmetric phugoid motion at low angle of attack. This phugoid motion is considered sufficiently controllable by pilot input. Thus, in the simulator experiments, the bang-bang inputs are given as instructions to recover the angle of attack.

4. Pilot-in-the-Loop Simulation

4.1 Experimental Method

In the real-time simulator experiments, the aircraft is piloted by a former airline pilot who has operational experience with commercial aircraft, including the Boeing 747 and Boeing 737. The input hardware consists of a yoke (δ_e and δ_a), rudder pedals (δ_r), and a throttle lever (δ_T), as shown in Fig. 3. These inputs are reflected in the numerical integration of the equations of motion in the in-house code. For visualization, the commercial flight simulator software X-Plane 11 is used. The flight instruments and the external view from the cockpit are displayed on a screen, as shown in Fig. 4.



Figure 3 – Flight simulator setup.

In addition, a stall warning sound is activated when $\alpha > 10$ deg. (The stall angle of this model is $\alpha \simeq 10$ deg [9].)
This paragraph describes the equations of motion used in the simulator experiments. For visualization purposes, the state variables x_e, y_e, and ψ are added. In addition, the throttle command δ_T is included as an input. Thus, the system is expressed as follows [7].

$$\begin{aligned} \dot{\boldsymbol{x}} &= \boldsymbol{f}(\boldsymbol{x}, \boldsymbol{u}) \\ \boldsymbol{x} &= [x_e, y_e, z_e, \phi, \theta, \psi, U, V, W, P, Q, R]^T \\ \boldsymbol{u} &= [\delta_r, \delta_a, \delta_e, \delta_T]^T \end{aligned} \tag{10}$$

The dynamics is computed at the GTM scale and then converted to the full scale for output. In addition, throttle input is considered in the simulator experiments. Thrust variation is expressed as $-100\ \% < \delta_{\mathrm{T}} < +100\ \%$ relative to the level-flight condition of the GTM. As this is a preliminary study, engine dynamics is ignored, and the thrust is assumed to respond instantaneously to the throttle lever input.
This paragraph describes the details of the experiments. The initial condition is the stable equilibrium point corresponding to deep stall, and the initial altitude is set to $10{,}000$ m. The objective is to recover the aircraft to the level flight. We conduct three experimental cases as follows: pattern 1 (manual input without instructions), pattern 2 (manual input with text instructions), and pattern 3 (automatic input). To reduce the influence of pilot learning, pattern 1 is performed before pattern 2, and pattern 2 is performed before pattern 3.
In pattern 2, the text instructions shown in Fig. 5 are displayed in the upper-right corner of the screen immediately after the simulation starts. These instructions are based on the bang-bang inputs shown in Fig. 2c. Here, from Eq. (3), the 0.5 s input duration at the GTM scale corresponds to 2.13 s at the full scale. However, for simplicity, it is approximated as 2.0 s in the simulator experiments.
In pattern 3, the bang-bang inputs are automatically executed 10 s after the start of the simulation. The bang-bang inputs are expected to reduce the angle of attack, and the pilot is required to achieve convergence of the phugoid motion.



Figure 4 – Simulator display.

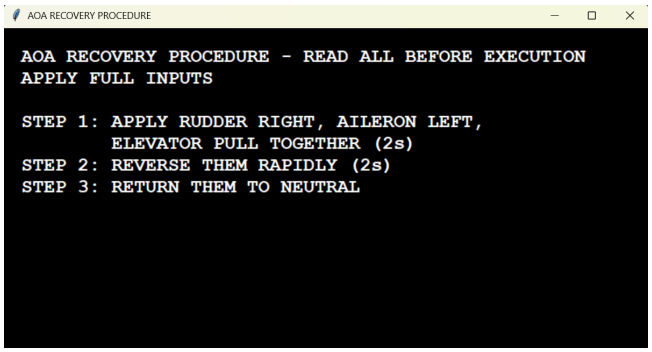


Figure 5 – Text instructions.

4.2 Result of Pattern 1 (manual input without instructions).

Figure 6 shows the typical result of pattern 1, manual input without instructions. The aircraft did not recover from deep stall, resulting in a $10{,}000$ m altitude loss and a crash. According to the pilot's comments, the pilot attempted to stop the yaw rate with the rudder, correct the roll angle with the ailerons, and push the elevator. In other words, the strategy was to lower the angle of attack while maintaining a symmetric flight condition. However, in a deep stall condition, the elevator control authority is not sufficient and this attempt failed.

The simulation results in Figs. 6b and 6c support the pilot's comment. The elevator δ_e remains pushed for most of the time. The lateral variables oscillate around 0. Furthermore, ailerons δ_a and roll angle ϕ tend to have the same sign, which indicates an intention to generate counter moment. Also, rudder δ_r and yaw rate R have a similar trend.

4.3 Result of Pattern 2 (manual input with text instructions).

Figure 7 shows the result of the first trial of patten 2, manual input with text instructions. At $t = 0$ s, the text instructions shown in Fig. 5 were displayed, and the pilot started control input at $t = 12$ s. The angle of attack decreased around $t = 30$ s, and the aircraft subsequently converged to level flight. The altitude loss was approximately $5{,}500$ m.

This paragraph examines the pilot's bang-bang inputs in detail, dividing them into the first half and the second half. In the first half, the control inputs (δ_r, δ_a, δ_e) were not applied simultaneously, but are applied in the order in which they appear in the text instructions: rudder, ailerons, and elevator. Furthermore, the input durations were approximately 10 s, which were longer than the duration of 2.0 s specified in the instructions. In the second half, the rudder and aileron inputs were applied in the opposite direction to those in the first half for approximately 3.0 s, but the elevator was not reversed. These results suggest that the pilot workload was high, leading to the reduced reproducibility of

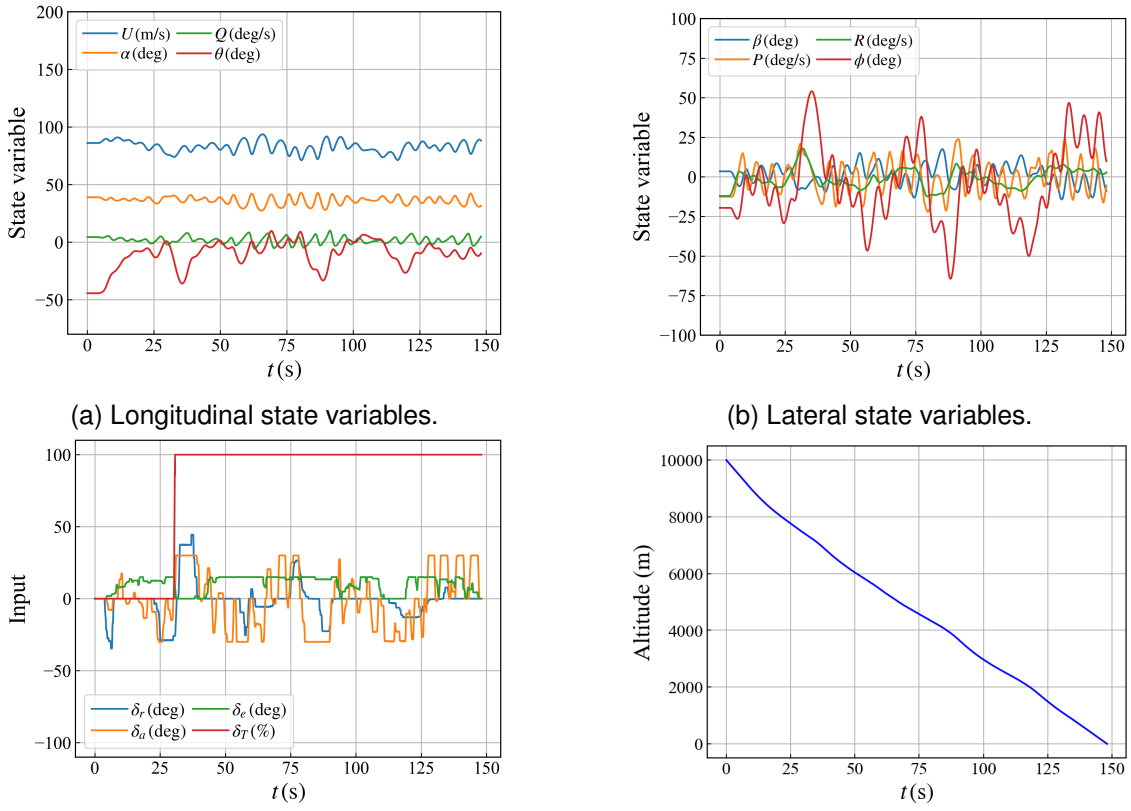
control inputs. On the other hand, despite such input errors, reduction of the angle of attack was achieved. This suggests that the bang-bang inputs may be robust against input errors to some extent.
The pilot commented that recovery of airspeed and attitude after reduction of the angle of attack was straightforward and did not differ significantly from normal flight operation.

4.4 Result of Pattern 3 (automatic input).

Figure 8 shows the result of the first trial of patten 3, automatic input. At $t = 10$ s, the automatic input began, and the angle of attack decreased immediately. Subsequently, the aircraft converged to level flight by pilot manual inputs. The altitude loss was approximately $3{,}000$ m. In addition, the altitude loss after the start of the automatic input was approximately $2{,}000$ m. From $t = 87$ s, the pilot adjusted the flight-path angle using the throttle input δ_T, which indicates sufficient temporal and cognitive margins. These results suggest that, by using automatic input to reduce the angle of attack, recovery to level flight can be achieved without significant workload. In addition, the altitude loss is smaller than that with manual input.

5. Conclusion

In this paper, first, we obtain the optimal recovery from the stable equilibrium point with deep stall of a T-tail airliner. The optimal input utilizes the coupling of longitudinal and lateral dynamics. Then, we simplify the optimal input as bang-bang inputs, and use them as text instructions to the pilot or automatic inputs in the real-time simulator experiments.
The three experimental cases were conducted as follows: pattern 1 (manual input without instructions), pattern 2 (manual input with text instructions), and pattern 3 (automatic input). In pattern 1, the pilot attempted to reduce the angle of attack using the elevator while maintaining a symmetric flight condition. However, this only led to a symmetric deep stall condition, because of the loss of elevator control authority in deep stall. In pattern 2, deep stall recovery was achieved through manual input based on the text instructions. However, the result also indicated that the pilot workload was high and



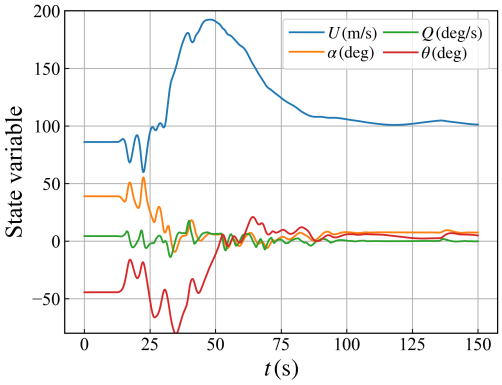
(a) Longitudinal state variables.

(b) Lateral state variables.

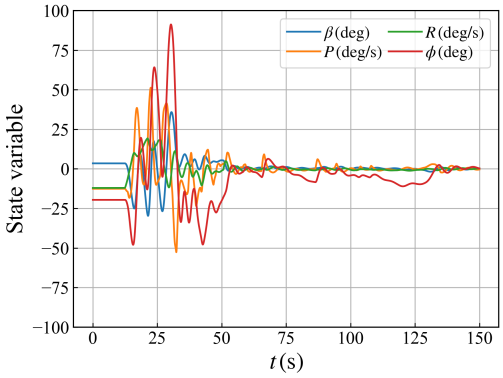
(c) Control inputs.

(d) Altitude.

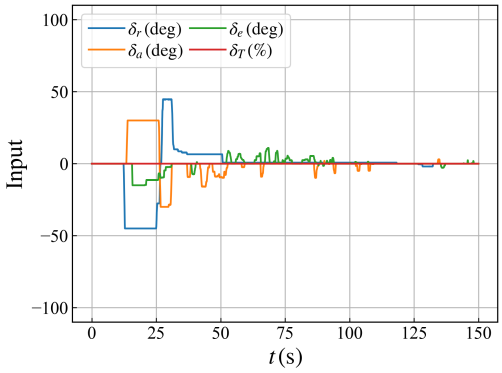
Figure 6 – Result of pattern 1, manual input without instructions (at full scale).



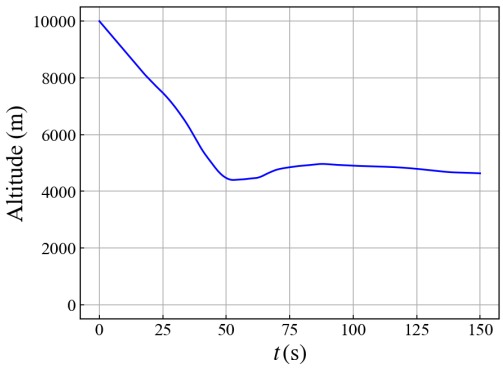
(a) Longitudinal state variables.



(b) Lateral state variables.

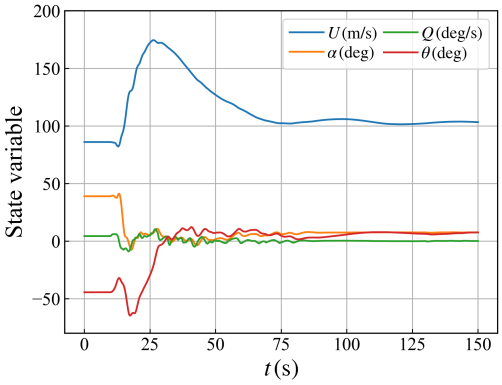


(c) Control inputs.

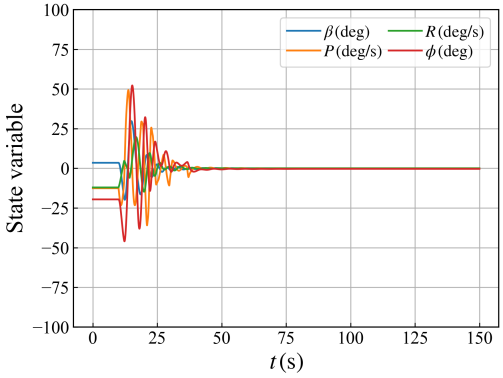


(d) Altitude.

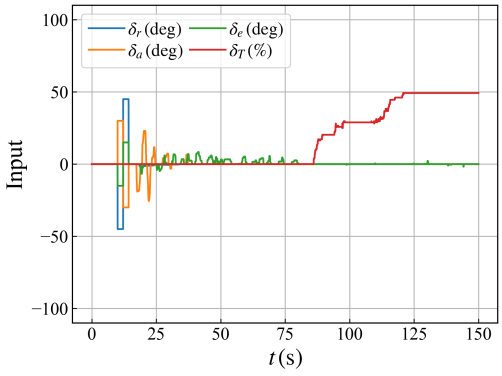
Figure 7 – Result of pattern 2, manual input with text instructions (at full scale).



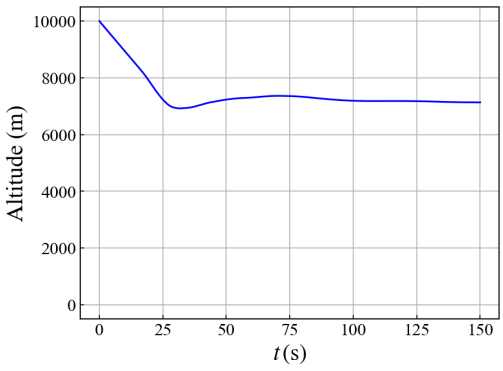
(a) Longitudinal state variables.



(b) Lateral state variables.



(c) Control inputs.



(d) Altitude.

Figure 8 – Result of pattern 3, automatic input (at full scale).

the reproducibility of the inputs remains an issue. In pattern 3, more rapid deep stall recovery was enabled by the automatic bang-bang inputs with lower pilot workload.
Some future directions are discussed below. First, pilot workload should be considered in the optimal control problem. For example, constraints on the number of control surfaces operated simultaneously could be introduced. Second, alternative methods for providing input instructions to a pilot with lower workload than text instructions should be explored. One possible candidate is a visual guidance method similar to a flight director.

6. Appendix: Specific Values of Stable Equilibrium Points

This section provides the stable equilibrium points at the GTM scale. Here, $\boldsymbol{x} = [\phi, \theta, U, V, W, P, Q, R]^T$.
Level flight

$$\begin{cases} \boldsymbol{x} = [0.00\ \text{deg}, 4.00\ \text{deg}, 24.1\ \text{m/s}, 0.00\ \text{m/s}, 3.17\ \text{m/s}, 0.00\ \text{deg/s}, 0.00\ \text{deg/s}, 0.00\ \text{deg/s}]^T \\ [\alpha, \beta]^T = [7.47\ \text{deg}, 0.00\ \text{deg}]^T \end{cases} \tag{11}$$

Flat spin with deep stall

$$\begin{cases} \boldsymbol{x} = [-18.2\ \text{deg}, -45.0\ \text{deg}, 20.1\ \text{m/s}, 1.65\ \text{m/s}, 16.3\ \text{m/s}, -57.5\ \text{deg/s}, 17.9\ \text{deg/s}, -54.5\ \text{deg/s}]^T \\ [\alpha, \beta]^T = [39.1\ \text{deg}, 3.66\ \text{deg}]^T \end{cases} \tag{12}$$

7. Contact Author Email Address

koki-yoshioka@g.ecc.u-tokyo.ac.jp

8. Copyright Statement

The authors confirm that they, and/or their company or organization, hold copyright on all of the original material included in this paper. The authors also confirm that they have obtained permission, from the copyright holder of any third party material included in this paper, to publish it as part of their paper. The authors confirm that they give permission, or have obtained permission from the copyright holder of this paper, for the publication and distribution of this paper as part of the ICAS proceedings or as individual off-prints from the proceedings.

References

[1] Nguyen DH, Lowenberg MH, and Neild SA. Derivation of control inputs for deep stall recovery using nonlinear frequency analysis. *The Aeronautical Journal*, 127(1308):232–254, 2023.

[2] Kolb S, Montagnier O, Hétru L, and Faure TM. Real-time detection of an aircraft deep stall and recovery procedure. *Journal of Guidance, Control, and Dynamics*, 42(5):1185–1194, 2019.

[3] Yoshioka K, Morita N, and Tsuchiya T. Stall recovery method with optimal control for t-tail transport aircraft and evaluation in monte carlo simulation. In *AIAA SCITECH 2026 Forum*, 2026.

[4] Yoshioka K, Morita N, and Tsuchiya T. Analysis on steady state with deep stall of t-tail transport aircraft and optimal recovery control. *Journal of the Japan Society for Aeronautical and Space Sciences*, 73(6):249–259, 2025 (in Japanese).

[5] Nguyen LT, Ogburn ME, Gilbert WP, Kibler KS, Brown PW, and Deal PL. Simulator study of stall/post-stall characteristics of a fighter airplane with relaxed longitudinal static stability. NASA TP-1538, 1979.

[6] Montgomery RC and Moul MT. Analysis of deep-stall characteristics of t- tailed aircraft configurations and some recovery procedures. *Journal of Aircraft*, 3(6):562–566, 1966.

[7] Kato K, Ohya A, and Karasawa K. *Introduction of Aircraft Dynamics*. University of Tokyo Press, Tokyo, 1982 (in Japanese).

[8] Jordan T, Foster J, Bailey R, and Belcastro C. Airstar: A uav platform for flight dynamics and control system testing. In *25th AIAA Aerodynamic Measurement Technology and Ground Testing Conference*, 2006.

[9] Soderman PT and Aiken TN. Full-scale wind-tunnel tests of a small unpowered jet aircraft with a t-tail. NASA TN-D-6573, 1971.

[10] NASA. Gtm_designsim. `https://github.com/nasa/GTM_DesignSim`, 2019. [retrived 13 Jun. 2024].

[11] Hueschen RM. Development of the transport class model (tcm) aircraft simulation from a sub-scale generic transport model (gtm) simulation. NASA TM–2011-217169, 2011.

[12] Benson DA, Huntington GT, Thorvaldsen TP, and Rao AV. Direct trajectory optimization and costate estimation via an orthogonal collocation method. *Journal of Guidance, Control, and Dynamics*, 29(6):1435–1440, 2006.

[13] Garg D, Patterson M, Hager WW, Rao AV, Benson DA, and Huntington GT. A unified framework for the numerical solution of optimal control problems using pseudospectral methods. *Automatica*, 46(11):1843–1851, 2010.

[14] COIN-OR. Ipopt. `https://github.com/coin-or/Ipopt`, 2024. [retrived 2 Nov. 2024].